The Effect of Electromagnetic Pressure on Silicon Wafer Manufacturing

Major Qualifying Project Report

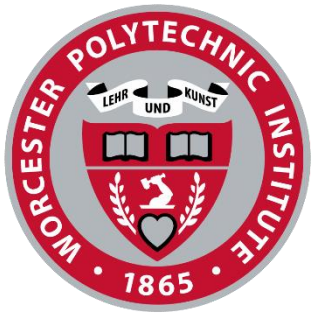

WPI

A Major Qualifying Project is submitted to the faculty of

WORCESTER POLYTECHNIC INSTITUTE

in partial fulfillment of the requirements for the Degree of Bachelor of Science

Submitted to:

Prof. Adam C. Powell

Worcester Polytechnic Institute

Submitted by:

Mason Vega

Date:

December 16th, 2022

Table of Contents

Abstract

In this research, a new manufacturing process for creating silicon crystal substrates is proposed. It differs from conventional plate solidification processes in the utilization of electromagnetic whose goal is to reduce the substrate thickness while it is being continuously pulled from the liquid material in the crucible. This research utilizes an alloy mixture of bismuth and indium instead of silicon due to the hazards and reactive nature of liquid silicon. In previous studies conducted at Shibaura Institute of Technology, several initial conditions of the electromagnetic pressure were unsuccessful at creating large areas of ultra-thin cross sections. This study focused on the application of frequencies at 2.5 MHz and 630 kHz to thin the solidifying metal alloy substrates as well as the use of thermal Finite Element Analysis to simulate the process and estimate the optimal rate of forced convection heat transfer on the system. By using the simulated heat transfer coefficient as a starting point for the cooling units, keeping the solidification line of the substrate centered under the electromagnetic coils was easier. By running the experiments through a variety of voltage variations, multiple successful combinations of frequencies, voltages, and magnetic flux densities were found that created substrates with thickness less than 100 micrometers in larger areas than prior studies.

0. Introduction

Throughout the past few decades, the interest in renewable sources of energy has grown while the world has started to see the impacts of global warming on a large scale. While the use of fossil fuels has started to slowly be phased out, renewable energy options have not yet been able to handle the demand that will be required. All of the different modes of renewable energy sources have their benefits like being able to supply power to off the grid residences and drawbacks like lack of accessibility or geographically unavailability.

Hydroelectric options take the kinetic energy from moving water and transfer it into usable energy. This can be seen in hydroelectric dams utilizing flowing water, facilities pumping storage water which induces a kinetic energy feedback, and ocean tidal power harvested from the motion of the waves. Even though quite powerful, hydroelectric facilities can be very region dependent and require access to large quantities of water.

Wind energy relies heavily on the use of turbines to generate power. It often has some difficulty competing with the cost of other renewable and non-renewable sources of energy in locations that do not produce ample amounts of wind. Although wind farms filled with turbines provide a large amount of energy and jobs to communities, they are only viable for use in specific sites (Stankovic et al., 2009).

Solar energy is the most abundant form of renewable energy compared to wind, hydro-electric, geothermal, bioenergy, and a few others. The US Department of Energy estimates that in just one hour, the total energy from the sun that hits the surface of the earth is more than enough for humankind's energy consumption for 1 year (Tsao, 2006). Although being able to absorb that much energy for human use is unrealistic, that statistic points out the ceiling of what can be achieved with solar energy technology.

Although abundant, solar energy technology is costly and often more complicated than kinetic energy farming methods like wind and water. With the sun's energy being semi-permanent and nearly infinite in scale, large leaps in technology or cost reductions of the materials can make harvesting more cost effective. This report concerns the fabrication of silicon crystal substrates, often called wafers, from liquid silicon, which is one of the main material process steps in solar panel manufacturing. They are usually produced by casting ingots from molten silicon, and cutting them into thin wafers. This method can be costly, while wasting considerable value high-purity silicon. This report aims at documenting and improving an ongoing research study that is trying to solve some of the issues relating to the current method of producing silicon crystal substrates.

Currently the Czochralski and CAST methods are the most widely used process for manufacturing single-crystal silicon substrates. The Czochralski method is used to generate single crystal substrates for a variety of metals and semiconductor materials. A seed material is used to grow and pull the single crystal ingot out of the associated liquid in a heated crucible. This single crystal ingot of silicon can then be cut into wafers and post processed. The CAST method differs by making polycrystalline ingots in a mold and then cutting them into wafers (Goetzberger et al., 2003). Both of these processes create waste material from cutting the ingots and the wafers can range from 0.75 - 0.2 mm. This report aims at documenting and improving an ongoing research study that is trying to solve some of the issues relating to the current method of producing silicon crystal substrates.

The method proposed for creating single crystal silicon wafers in this research differs in its use of electromagnetic pressure on the region of the molten material undergoing solidification into the wafer. This proposed method relies on the surface tension of the liquid material to produce the thin wafers directly and continuously, without the need to cut down a full ingot. The added electromagnetic pressure aims to thin the wafers more drastically, under 0.1mm, to allow for application to solar panels

that can be mounted on curved surfaces (Hanoka, 2001). These thinner and efficiently produced wafers could open up more possibilities for the creation and use of flexible solar panels in the future.

Because of challenges in the melting temperature and environment conditions required to generate silicon crystals, model experiments have been created using the U-72 alloy consisting of Bismuth and indium. This material was chosen for its lower melting point of 72 degrees Celsius and its lack of reactivity under laboratory conditions. The aim of the following project is to validate that this process can create single crystal substrates of U-72 that are less than 0.1mm thick through the laboratory experiments and thermal analysis simulations using ANSYS. Based on results that demonstrate the effectiveness of electromagnetic pressure on this crystal substrate production method for U-72, more research can further explore the effect, followed by pure silicon crystal wafer production using this method.

1. Background and Literature Review

2.1 History of Solar Power

Technically, the power of the sun has been utilized in many ways throughout the history of mankind. In as early as 3rd century B.C. magnifying glass like materials and mirrors were used to light torches and ceremonial items (Rossi & Russo, 2017). Sunrooms are also a concept that is still being used today which utilizes the suns energy. Usually they are south facing rooms with large windows that let ample amount of sunlight into the room allowing it to stay warmer in colder months, or in the case of the ancient Romans to heat their bathhouses.

The concepts of modern solar panels were realized much later throughout the 19th century. Edmond Becquerel is one of the first credited for the invention of the solar cell (Fraas, 2014). He

determined that he could generate electricity when two electrodes were placed in a conducting solution and exposed to sunlight. This concept is now known as the photovoltaic effect.

The first version of solar panels were made with the element of selenium. In 1883 Charles Fritts produced the first consistent solar cells made from selenium wafers (Fraas, 2014). This creation was a large step forward in the direction of manufacturing solar cells. Today, modern solar cells are made out of silicon as the main element. This change is often credited to Daryl Chapin, Calvin Fuller, and Gerald Pearson's creation of the silicon photovoltaic (PV) cell at Bell Labs in 1954 (Goetzberger et al., 2003). Many argue that this event marks the true invention of PV technology because it was the first instance of a solar technology that could actually power an electric device for several hours of a day. Although operational, they converted sunlight at 4% efficiency, which is less than a sixth of what modern single crystal silicon photovoltaic cells can generate today (Markvart & Castañer, 2018). Figure 1 below displays the trends of estimated efficiencies for different photovoltaic technologies over the years (*Best-Research-Cell-Efficiencies-Rev220630.Pdf*, 11/28/2022). The blue markers identify the methods that utilize single crystal silicon wafers.

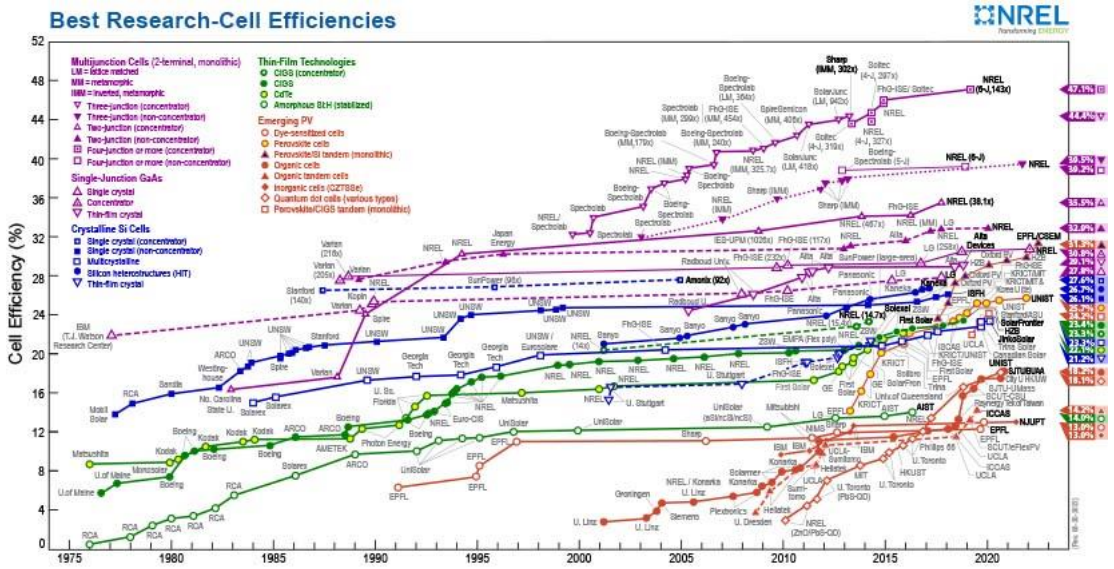

Figure 1: NREL Conversion Efficiencies for Photovoltaic Technologies Throughout History

2.2 Solar Cell Operation

The photovoltaic (PV) energy conversion process in solar cells can be simplified into two steps. Initially, the absorption of light generates an electron-hole pair, then the electrons and holes are separated. The electrons and holes are sent to apposing terminals, through the depletion zone, generating electricity (IBID). The solar cell has a layer of n-type silicon and p-type silicon sandwiched together. In between is the stated depletion zone which allows the electrons to be able to fill the holes on the silicon substrate on the other side. Once the electrons have crossed through and filled the holes in the depletion zone they create an internal electric field that prevents electrons from the n-type layer to fill the p-type layer. Sunlight hitting the PV panels causes the silicon to eject the electrons. The created electric field will move the locations of the electrons and the holes. If the layers are connected by a conducting wire the electrons will travel between layers, through the depletion zone, and into the wire creating a flow of electricity. This process can be seen from Figure 2.

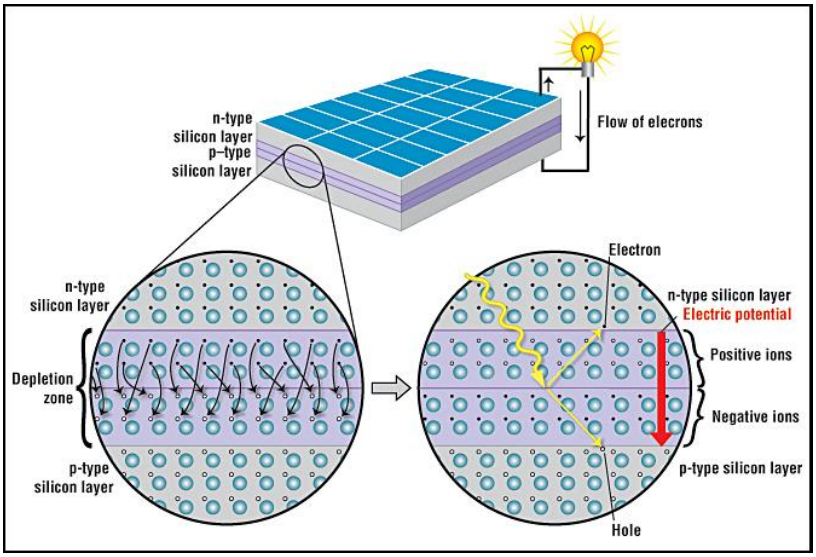

Figure 2:Schematic representation of a solar cell, showing the n-type and p-type layers, with a close-up view of the depletion zone around the junction between the n-type and p-type layers. (Fernandez, 2013)

A single PV cell is quite small, producing about 1-2 watts of power. The cells dealt with in this research are mostly made of mono and multi-crystalline silicon. These thin sheets of silicon are sandwiched between different forms of glass and polymers for protection inside of a solar panel. Said solar panels are a combination of many PV cells connected or chained together in modules. Modules can be used individual, or for larger scales of operation and can be connected together to form arrays. These arrays would then be connected to the electrical grid as a part of a complete solar panel system. This modularity is very useful in order to solve problems of scale. They can be combined to meet the needs for specific uses as long as the user has the ability to store the energy or sell it directly to the grid.

2.3 Single-Crystal Silicon Substrate Manufacturing

Due to factors like cost, access, and research conducted, only multi-crystalline silicon and monocrystalline Czochralski (Cz) crystals are the primary silicon substrates used in PV cells (Goetzberger et al., 2003). This process was discovered by Jon Czochralski in 1916 and used to grow large silicon crystals used for semiconductors, PV wafers, microchips, etc. The process creates larch cylindrical ingots that can be thinly sliced and used in microelectronics and PV cells. Initially the process was only used to observe the crystal growth rates of some metals, but in 1950 Bell Telephone Laboratories rediscovered the process for mass production of single crystal ingots (Stefano, n.d.). There is also a process called Ohno Continuous Casting that is utilized to create single crystal ingots of aluminum and tin horizontally and vertically (Ohno, 1986). The goal of this process was to create mono-crystalline ingots by eliminating the possibility of crystals growing on the walls of the mold by having the walls heated above the metals solidification point. This research has been very successful for producing mono-crystalline wires and ingots of Al and Sn, but was not utilized for Silicon.

For manufacturing silicon wafers, the large single-crystal ingots are grown at 200 – 300 mm in diameter and can reach lengths of 2 meters. A seed crystal is inserted into the molten silicon. Boron or phosphorus can be added to dope the silicon turning them into p-type or n-type material as mentioned in the solar cell operation section. The seed is precisely lifted out of the molten material spinning at a constant speed growing a single-crystal silicon ingot. These extractions are usually performed in an atmosphere of an inert gas, like argon, to present the silicon from reacting with the oxygen in the air. Once finished the cylindrical crystal ingot can be cut into silicon wafers.

Some issues with the method relate to the waste and impurities produced with the ingot. The process generally utilizes a quartz crucible that can slowly dissolve into the molten silicon adding oxygen into the ingot. Too much oxygen contamination in the crystal can have detrimental effects on the electrical conductivity of the wafers after being cut. Secondly, the cutting of the wafers leaves behind the edges of the ingot, which creates waste that is can no longer be used for that batch of wafers.

2. Methodology

3.1 ANSYS Thermal Finite Element Analysis Simulation

Ansys is a suite of software products that can simulate a variety of engineering environments around fluid dynamics and thermal analysis and output results. This research primarily uses it for its thermal analysis capabilities to model the heat transfer through the experiment rig as well as to determine the cooling capacity needed to stabilize the solidification line when producing the substrate.

First the physical model of the crucible, liquid substrate, and seed plate are uploaded into the software. The surfaces and volumes of these models are assigned their properties when the specific material is added from the library. For example, the solid seed plate has a high thermal conductivity as it

is made out of copper. The states of all the surfaces are identified and added to the overall mesh. At this point the environment settings are added. This would include the energy exerted from the heater, coil cooling unit, and the general room temperature. Figure 3 displays the model within Ansys.

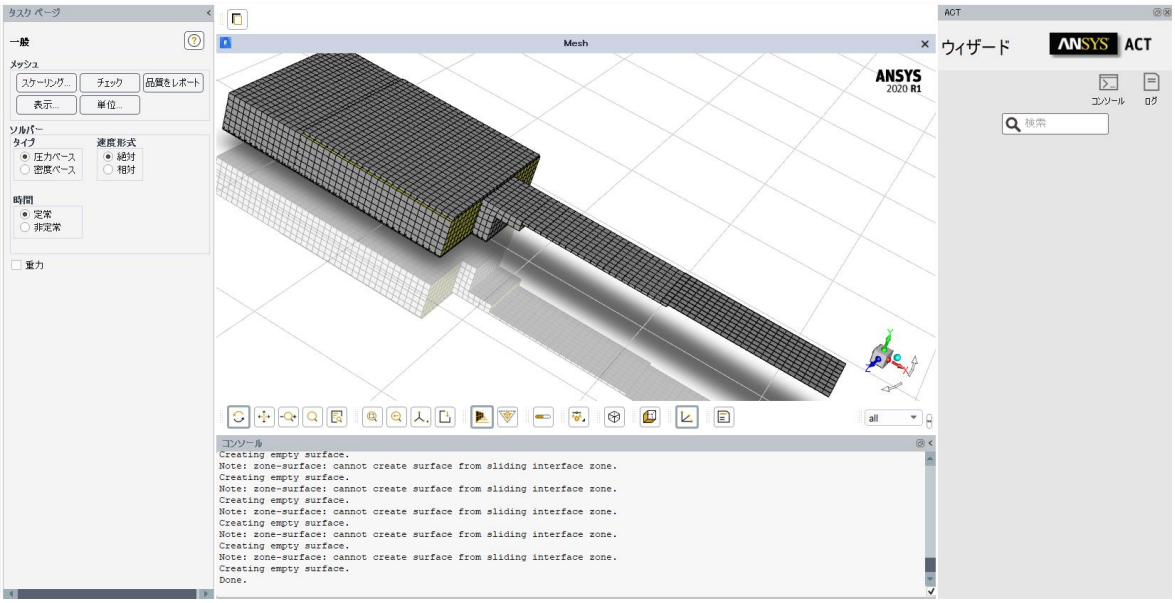

Figure 3: ANSYS CAD Model

After the models are composed, the parameters for the simulation are set. This includes settings like the error factor, size of the mesh, and number of times the simulation is run. The settings are initialized and when ran, they produce a map that displays the error of the first simulations and settles on the final results seen in Figure 4. When the models are now opened in the analysis section specific surfaces and bodies can be chosen to display their temperature heat maps. This temperature variation validates which conditions are needed to make sure the proper temperature for solidification, 72 degrees Celsius, is centered under the electromagnetic coils. When confirmed, the cold air velocity from the coil cooling unit can be set to ensure that the experiment to create the substrate doesn't fail.

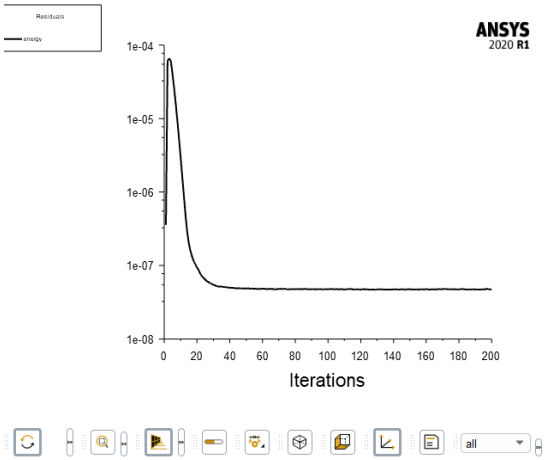

Figure 4: Simulation Error Plot

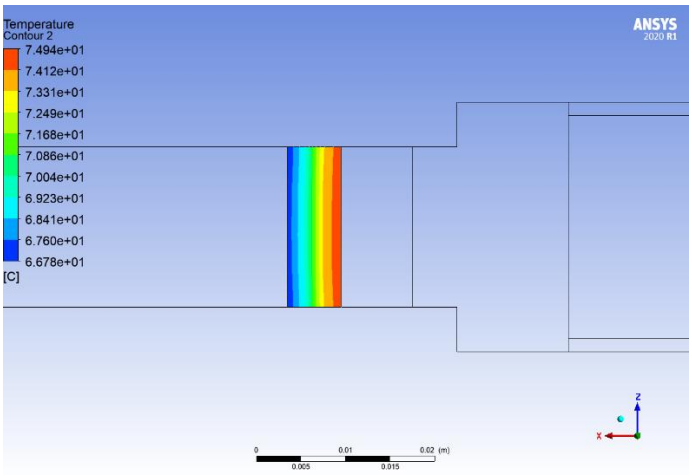

Figure 5: Solidification Temperature Simulation Result Example

3.1.2 Electromagnetic Pressure and Heat Generation Equations

The electromagnetic pressure applied to the solidifying metal thins the substrate from both sides. If the pressure is too high the opposing fields will cancel each other out, and if the field is too small they will not reach past the surface of the solidifying substrate. Figure 6 below displays the simplified cross section of the electromagnetic pressure process. The electromagnetic force has been calculated using Equation 1 below. The equation considers the decay of the magnetic field as it passes through the surface of the material to penetrate the center. The center of the substrate is through the z-axis and the material surface is defined as 0. This makes the interior material $z > 0$ from either direction.

This means that Equation 1 needs to be separated so that Equation 2 and Equation 3 generate the electromagnetic force from either side.

Equation 1

$$f = \frac{\mu_0 H_0}{2\delta} \mathrm{e}^{-\frac{2z}{\delta}} = \frac{B_0^2}{2\mu_0 \delta} \mathrm{e}^{-\frac{2z}{\delta}}$$

Equation 2

$$f_{upper} = \frac{B_0^2}{2\mu_0 \delta} \mathrm{e}^{-\frac{2}{\delta}(-y+\frac{t}{2})}$$

Equation 3

$$f_{lower} = -\frac{B_0^2}{2\mu_0 \delta} \mathrm{e}^{-\frac{2}{\delta}(y+\frac{t}{2})}$$

The effective electromagnetic force is the sum of the both of the equations. Once combined, they need to be integrated from the center of the plate thickness at y=0 to the surface of y=t/2 to find the electromagnetic pressure $P_m\,[\mathrm{Pa}]$. Equation 4 shows the combination of the forces from either side of center of the plate while Equation 5 shows the results after integration in pascals.

Equation 4

$$\begin{aligned} f &= f_{upper} + f_{lower} \\ &= \frac{B_0^2}{2\mu_0 \delta} \cdot \left(e^{\frac{2y}{\delta}} \cdot e^{-\frac{t}{\delta}} - e^{-\frac{2y}{\delta}} \cdot e^{-\frac{t}{\delta}} \right) \\ &= \frac{B_0^2}{\mu_0 \delta} \cdot e^{-\frac{t}{\delta}} \cdot \sinh\left(\frac{2y}{\delta}\right) \end{aligned}$$

Equation 5: Electromagnetic Pressure from Coils

$$P_m = \int_0^{t/2} f\, dy$$

$$= \frac{B_0^2}{2\mu_0} \cdot e^{-\frac{t}{\delta}} \cdot \left\{\cosh\left(\frac{t}{\delta}\right) - 1\right\}$$

$$P_m = 0.94\ [Pa]\ at\ 2.5 MHz, 12.0\ V, and\ 2.5\ mT$$

$$P_m = 0.95\ [Pa]\ at\ 630\ kHz, 8.0\ V, and\ 3.4\ mT$$

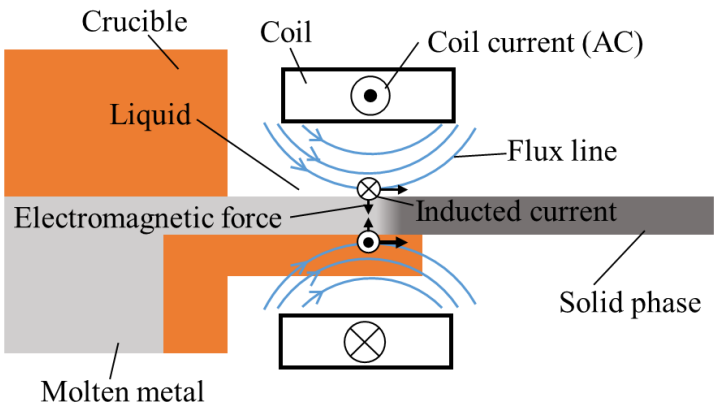

Figure 6: Electromagnetic Pressure Application Diagram

The understanding of the heat generated from this process is very critical to the success of the experiment. If the forced heat transfer by the cooling unit is too low the electromagnetic pressure severs the substrate at the solidification line, but if it is too high the substrate is fully solid before it has time to be affected by said pressure. The equations that are used from alloy U-72 to feed the ANSYS simulation can be found below.

Following the same coordinate system from the electromagnetic pressure equations, the center of the substrate is set at z with the surfaces at 0. The final equation for the heat generation coefficient is the integrated distribution of heat generation Q[$\mathrm{W/m^3}$] from the center of the plate thickness (y=0) to the plate surface (y=t/2) and dividing by half of the substrate thickness solves for the heat generation averaged in the thickness direction $\bar{Q}$ [$\mathrm{W/m^3}$]. This can be seen below in Equation 6.

Equation 6: Heat Generation Coefficient

$$\bar{Q} = \frac{2}{t}\int_0^{t/2} q\, dy$$
$$= \frac{2B_0^2}{\sigma\mu_0^2\delta t}\cdot e^{-\frac{t}{\delta}}\cdot\left\{\sinh\left(\frac{t}{\delta}\right)-\sin\left(\frac{t}{\delta}\right)\right\}$$

$$\bar{Q} = 1.43 * 10^7\left[\frac{W}{m^3}\right]\ at\ 2.5\ MHz, 12\ Volts, and\ 2.5\ mT$$

$$\bar{Q} = 7.84 * 10^6\left[\frac{W}{m^3}\right]\ at\ 630\ kHz\ , 8\ Volts, and\ 4.5\ mT$$

3.2 Alloy Wetting Experiment

One of the most important material properties for the liquid alloy in this experiment as well as the proposed end use of Silicon is the surface tension. The surface tension needs to be strong enough to connect the solid substrate with the liquid inside the crucible, while the liquid metal is also fluid enough to be manipulated by the imposed magnetic field. This type of experiment has been conducted on Silicon (Si) in order to understand the effect that temperature, vibrations, and other factors have on liquid Si being pulled from a silica crucible (Kanai et al., 2007). The study concluded that at ideal temperatures the wetting angle for Si on quartz glass is at 90° at 1,550°C, but at a slightly lower temperature of 1,500°C the angle was found to be 130°.

To mimic this experiment for the U-72 alloy a vacuum is not needed and the system only needs to reach 77°C. The experiment utilizes a heating pad that a droplet of the alloy U-72 will rest on. A camera setup takes a picture of the droplet sitting on top of the heating pad's surface, and a program will be utilized to calculate and average the wall angle over the course of multiple droplets. This setup can be seen below in Figure 7.

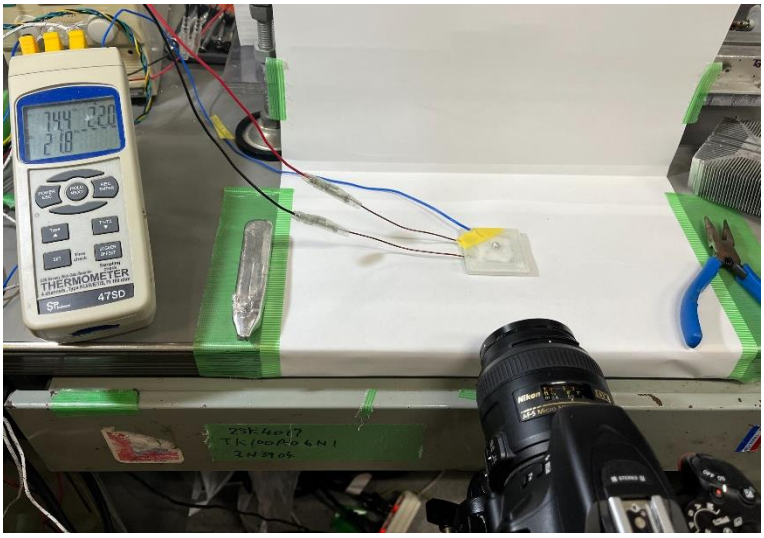

Figure 7: Wetting Experiment for Alloy U-72

The heating plate is brought to a temperature of 77.5 ± .4°C. It is measured with a temperature probe attached to the corner of the plate. Setup a camera so the focus is at the top face of the heating face. This will allow the drop of alloy to be visible in the frame once it touches the plate. Once the camera is setup and the heating plate is properly heated, the wetting experiment can take place.

Using a soldering iron, melt a droplet of alloy U-72 onto the heating plate. The droplet should be no larger than a pea and should weigh approximately .45 ± .1 grams. Once it lands near the center of the plate allow it settle for 1-2 minutes and focus the camera. Figure 8 displays what the camera monitor should look like before the photo is taken. Once the picture is taken, repeat the experiment multiple times with different droplets. Upload the photos into Image-j, or another image software, to measure

the angles between the top face of the heating plate and the sides of the droplet. Average the angles together to get the wetting angle of the experiment.

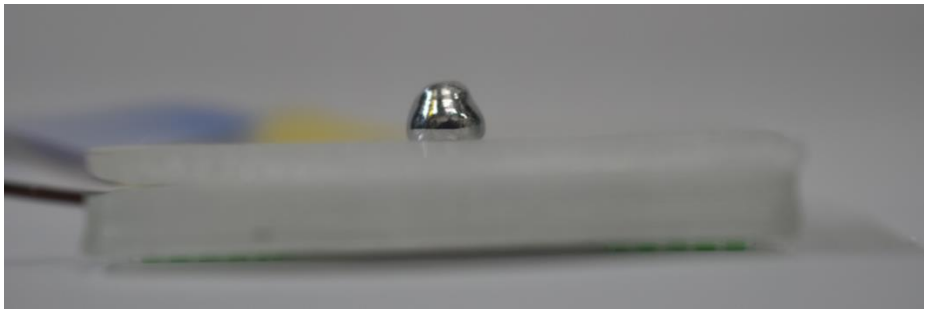

Figure 8: Wetting Experiment Camera Focus Example

3.3 Liquid Substrate Experiments

Although single-crystal silicon substrates are the main focus of the research, the current equipment is designed to run the experiments on alloy U-72 due to the limitations of the lab. The use of silicon for the current setup would require a much higher melting temperature as well as an oxygen free environment, essentially requiring the experiment to be completed in a vacuum. Alloy U-72 was chosen for its melting point at 72 °C. Based on information from the distributer, it is composed of 34% Bismuth and 66% Indium by weight and the main physical properties can be seen in Table 1 (Osaka Asahi Co., Ltd, Private Communication).

The overview of the experiment and test rig can be seen in Figure 9 and Figure 10 below. The alloy U-72 is brought above it's melting temperature in a crucible by a heater on the surface level. On the front of the crucible is a ramp that leads to an opening where a 0.1mm copper seed plate is inserted. Once the molten metal alloy is bonded with the edge of the seed plate, they are pulled out horizontally at a consistent speed. As the surface tension keeps the molten metal alloy bonded to the seed plate, the molten alloy is solidified by the outside air forming a thin single-crystal substrate. There is a ramp extending 9mm off the crucible to ensure that the substrate has enough time to solidify as it is pulled

out by the seed plate. Surrounding the ramp is the 3 turn coil that generates the electromagnetic pressure that is utilized during the second half of the experiment. Once 40mm of the substrate have properly solidified to the seed plate the coil is turned on to thin the substrate beyond nominal conditions. The coil is mounted around the crucible ramp where the solidification process is occurring. The experiment can be changed through 5 main variables: electromagnetic pressure frequency (Hz), electromagnetic pressure coil voltage (v), heat transfer coefficient (hf), experiment motor speed (s/rotation), and crucible temperature (°C). The electromagnetic coil being set at a frequency of 630 kHz or 2.5MHz is the most relevant variable determining the force at which the substrate is being squeezed from either side. The other 4 variables are observed as constants and can be adjusted to address specific concerns in the experiment. The experiment is completed when the crucible runs out of liquid alloy or a break or gap appears in the substrate. After this the new allow substrate is removed from the seed plate, the thickness distribution throughout it is observed and recorded. Figure 11 displays the substrate after completing a test experiment once the substrate is removed from the seed plate.

Table 1: Physical Properties of Alloy U-72

	Melting Point [°C]	Density (at 20.7°C) $[\frac{kg}{m^2}]$	Electrical Conductivity (at 24.0°C) $[\frac{1}{m*\Omega}]$	Surface Tension
Alloy U-72	72	$8.06 * 10^3$	$2.8 * 10^6$	

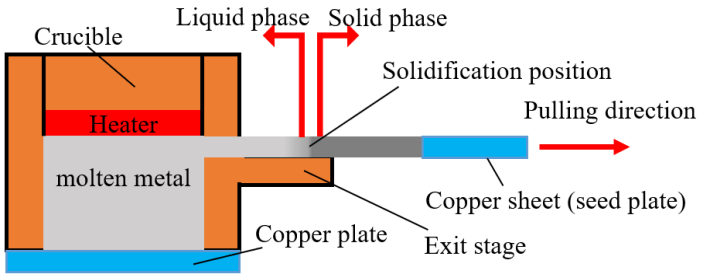

Figure 9: Experiment Overview

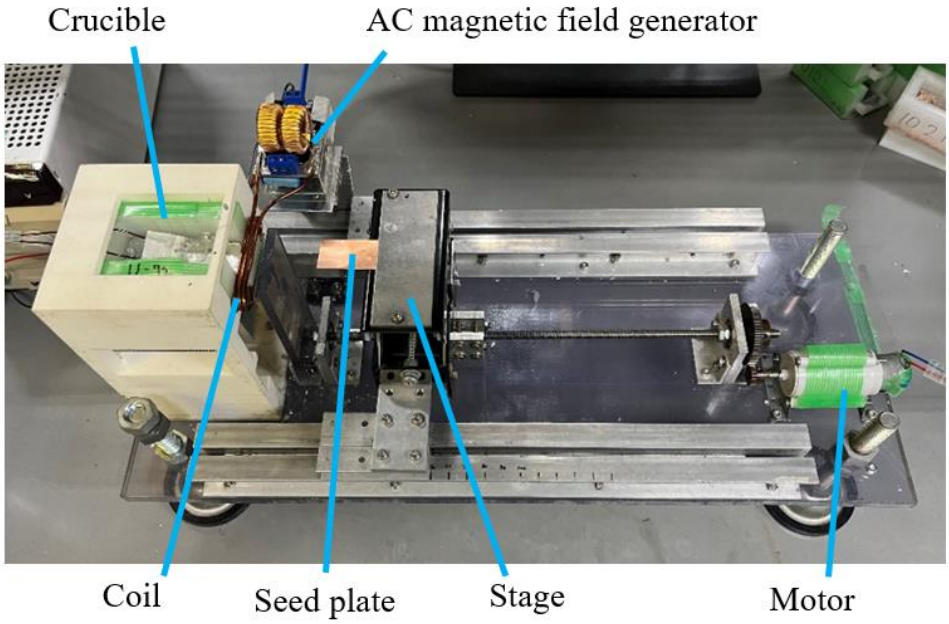

Figure 10: Experiment Test Rig

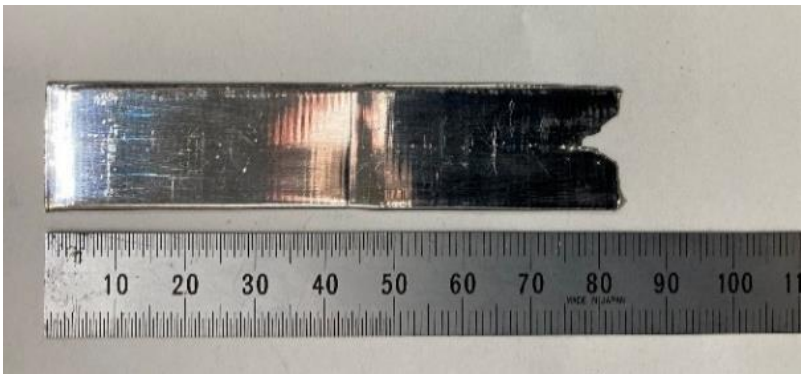

Figure 11: Sample Substrate Post Experiment

3.3.1 Experiment Setup

The experiment equipment utilizes a heating unit, motor, 3 fans, and an alternating electromagnetic current generator all powered by a logger. The voltages from these systems are displayed and recorded on a PC monitor behind the experiment setup. The logger is turned on followed by the power supplies for the motor, wave generator, heater, and fans. Before the experiment can be run the motor speed and electromagnetic current generator need to be tested to ensure that they are working at the expected levels.

Once powered up the electromagnetic frequency generator coils are attached to an oscilloscope. As seen below in Figure 12, the oscilloscope should be turned on using the auto set button. From there the wave pattern can be viewed. It should be a relatively smooth sinusoidal wave with an amplitude of 22.7 V. The voltage reading of the coils should be set to 630 KHz or 2.5MHz, depending on which version of the experiment is being run. If the sine wave on the oscilloscope is fuzzy or has an introduction of noise, it may be an indication that the electromagnetic frequency generator board is struggling to hold the frequency and may need to be replaced.

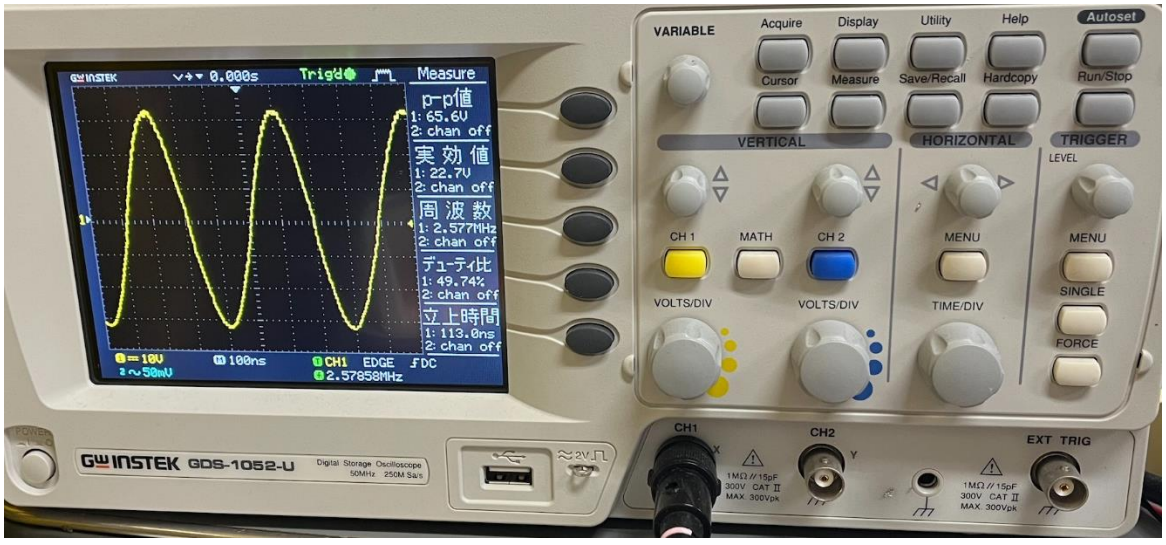

Figure 12: Oscilloscope Reading from Electromagnetic Wave Generator

The experiment rig is driven by a small DC motor powered by its own power supply. The motor is attached to a small gearbox that makes the final worm gear make 1 rotation about every 13-16 seconds. This system can be seen in Figure 13. To setup the motor we detach it from the driving mechanism and send it a constant voltage of 100 volts. A simple time study is conducted to determine the current speed of the motor by counting the rotations in 1 minute. After the first minute we adjust the voltage to get our ideal speed for that experiment. Increasing the voltage increases the speed. Once the ideal speed is determined and set we lock the motor back to the driving mechanism and shut off the voltage being sent from the power supply. The motor is now ready for the experiment.

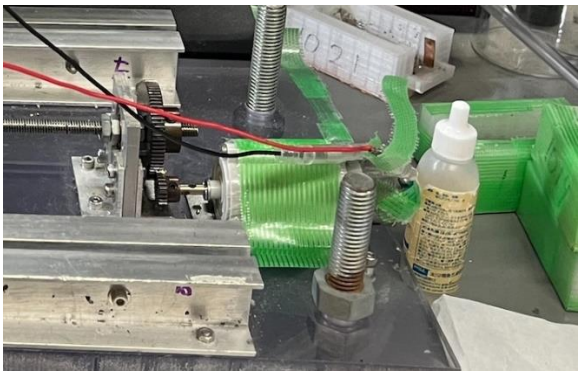

Figure 13: Motor Driven System

Once the mechanical systems are working and set for the experiment the seed plate can be prepped, secured, and set in the crucible. The copper seed plate is cut from a 0.1mm sheet. The seed plate is 20 mm by 50mm. The 20 mm edge that is going to bind to the liquid alloy is first cleaned with a dab of flux on both sides. This corrosive acid is meant to rid the surface of any impurities to allow the best chances for the alloy to properly bind. The edge that was not cleaned is fastened into the clamp that is pulled by the worm gear. The clamp and seed plate are then manually positioned so that the cleaned edge is just touching the liquid alloy. Once the plate is level, the motor can be locked into place and the experiment is ready to begin.

3.3.2 Applying Electromagnetic Pressure

After the experiment has been running on its nominal procedure for about 10-11 minutes, the substrate should be around 40mm in length. It is at this time that the electromagnetic pressure is to be applied. Before the coils are turned on the cooling fan system is set up. This system in necessary in order to keep the solidification line inside the electromagnetic coils. When turned on the coils release excess heat rapidly. If the cooling fan system is not turned on the solidification line is likely to move up the substrate and break the surface tension ending the experiment prematurely. The 2-fan system seen in Figure 14 runs on 12 volts each moving the chilled air about 1.2 - 4.2 m/s. This was found to be the ideal rate with the ANSYS simulations.

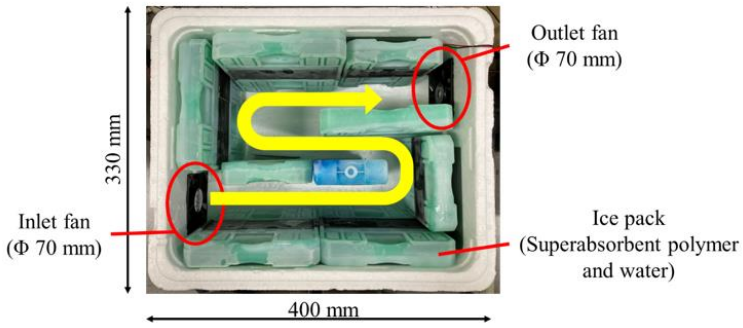

Figure 14: Fan Cooling System for Electromagnetic Coil

With the electromagnetic frequency generator and fan cooling system running the substrate should develop a clear line where the electromagnetic pressure was started. Due to unpredictable circumstances that are not possible to simulate it is important to pay attention to the solidification line to ensure that it stays inside the coils. If the solidification line starts to drift to far in or out the voltage running the fan cooling system can be throttled 1-2 volts in either direction. This experiment should last 25-50 minutes or until the substrates separates from the due to the low level of the liquid alloy. The

motor pulling the seed plate, the fans, and the electromagnetic frequency generator can now be turned off and the seed plate removed with the substrate attached.

3.2.3 Sample Collection and Documentation

With the seed plate and substrate removed from the experiment rig the process to observe, measure and record the data for the experiment can start. Firstly, the very end of the substrate touching the seed plate is cut off and separated. This ensures that all measurements taken do not include the thickness from the seed plate. A ruler is then used to mark every 5 millimeters down the center of the substrate. Using a micrometer, the thickness of each one of these center points are measured and recorded on a spreadsheet corresponding to the length at which they were found. There should be a noticeable decrease in thickness between the 40mm and 45mm mark.

From the 40mm location start marking points on either side of the center dot every 2 millimeters. Measuring these will show the varied thickness throughout the cross-section. Record these thickness readings in a chart similar to the one seen in Figure 15. The ideal substrate would have a large region with a thickness below 100 micrometers which has been determined to be needed in silicon wafers in order to create curved or flexible solar cells. If proven successful these experiments on the alloy U-72 could validate the process and further research testing for Silicon wafer production of a similar method.

20221130-4	−8	−6	−4	−2	0	2	4	6	8
630 kHz					0.72				
6.0v→7.25v					0.66				
Instant					0.576				
u-72					0.512				
					0.442				
					0.326				
					0.328				
	1.764	0.413	0.238	0.206	0.269	0.293	0.397	0.276	1.645
	1.657	0.347	0.041	0.016	0.057	0.144	0.122	0.247	1.499
	1.549	0.251			0.006	0.12	0.336	0.236	1.652
	1.392	0.337				0.093	0.226	0.189	1.506
	1.26	0.47					0.143	0.084	1.39
	1.108							0.006	1.342

Figure 15: Substrate Thickness Record Sheet Sample

3. Results

4.1 Simulation and Calculation Results

The heat generation coefficient was calculated using the equations found in section 3.3. For the current crucible and substrate size it was found to be $1.43 * 10^7 \left[\frac{w}{m^3}\right]$ at 2.5 MHz,12 Volts, and 2.5 mT and $7.84 * 10^6 \left[\frac{w}{m^3}\right]$ at 630 kHz ,8 Volts, and 4.5 mT. This is within reasonable limits and aligns to past experiments using differently sized substrates and crucibles.

Multiple thermal simulations were run for both the 2.5MHz and 630 kHz experiments. As depicted in Figure 16, the ideal outcome should have a temperature of 72 °C represented as the bring green section In the solidification line plot. The varying factor in the simulations was the forced heat transfer value. This value was increased by 5 until the optimal range on the line plot was found.

Seen in Figure 16, the forced heat transfer coefficient (hf $[\frac{W}{(m^2 \times K)}]$) was found to be 70 for the 2.5MHz simulation. A hf value of 80 was seen to be too high and did not allow the substrate to be affected by the magnetic field. Contrarily a hf value at 65 showed that the solidification line would be too far forward, likely causing the substrate to be severed by the electromagnetic pressure.

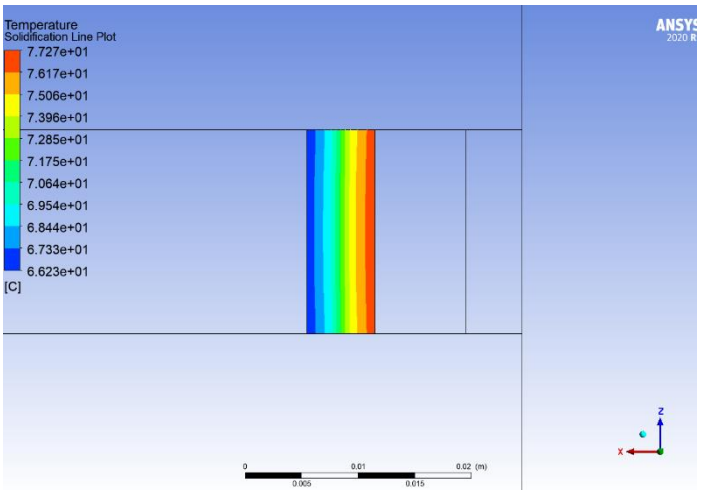

Figure 16: Solidification Temperature Simulation Results at 2.50 MHz at hf =

As shown in Figure 17, the forced heat transfer coefficient value was found to be 95 for the 630 kHz simulation. When at 100, the hf value was too high and did not allow the substrate to be affected by the magnetic field. Comparatively, hf at 90 showed that the solidification line would be too far forward and would likely sever the substrate by the electromagnetic pressure.

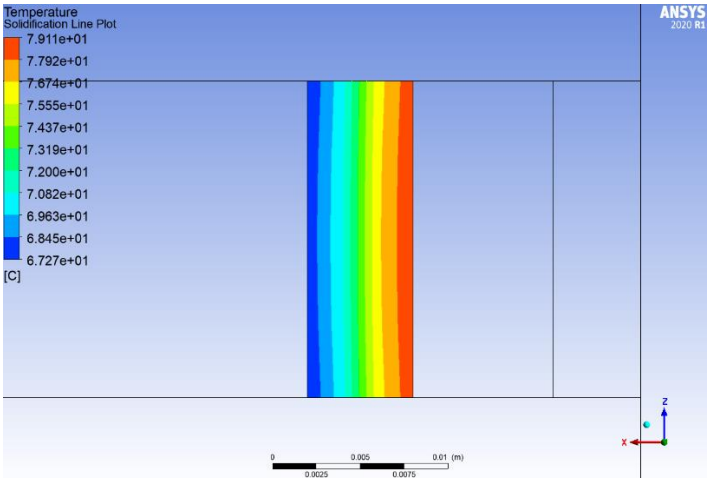

Figure 17: Solidification Temperature Simulation Results at 630 kHz at hf =

The Lorentz force formula is used in electromagnetism to understand the force exerted on an area that is moving through an electromagnetic field. This equation, as previously described in section 3.1.2, was calculated at different points along the y-axis of the substrate for both conditions and is depicted in Figure 18. These plots show the difference in the forces at the 2.5 MHz (a) and 630 kHz (b).

The higher frequency from the 630 kHz condition highlights the drastically larger electromagnetic fields that are formed from the coils.

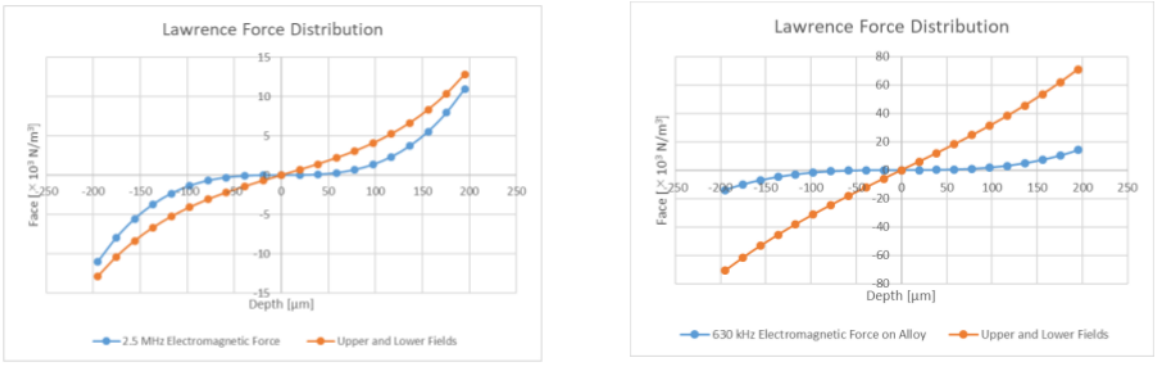

(a) (b)

Figure 18: Lorentz force Plot for the Conditions of (a) 2.5 MHz and (b) 630 kHz

Seen below in Table 2 are the important properties needed to compare alloy U-72 and silicon. These values are relative to the surface tension, magnetic, material, and conductivity property of the two metals. They are all either known values or formed from simple equations.

Table 2: Material properties and Dimensionless Number Values for Alloy U-72 and Silicon

Properties	Alloy U-72	Silicon
Melting Point	72°C	1,410 °C
Surface Tension [mN/m]	490	783.5
Density [kg/m^3]	8060	2330
Viscosity [mPa*s]	1.72	1
E. Conductivity [1/(Ω*m)]	2.8*10^6	1.2*10^6
Thermal Conductivity [W/(m/K)]	56.7	54.4
Specific Heat Capacity [J/(kg*K)]	195	858
Prandtl number	0.59 X 10^-2	1.58 X 10^-2
Weber Number	4.11 X 10^-9	0.74 X 10^-9
Capillary Number	1.76 X 10^-7	0.64 X 10^-7
Magnetic Reynolds number	1.76 X 10^-8	0.76 X 10^-8

4.2 Wetting Experiment Results

In Figure 19, a liquid droplet of alloy U-72 is sitting on a PLA heating plate. A series of these images was taken with different droplets for the U-72 wetting experiment described in section 3.2.

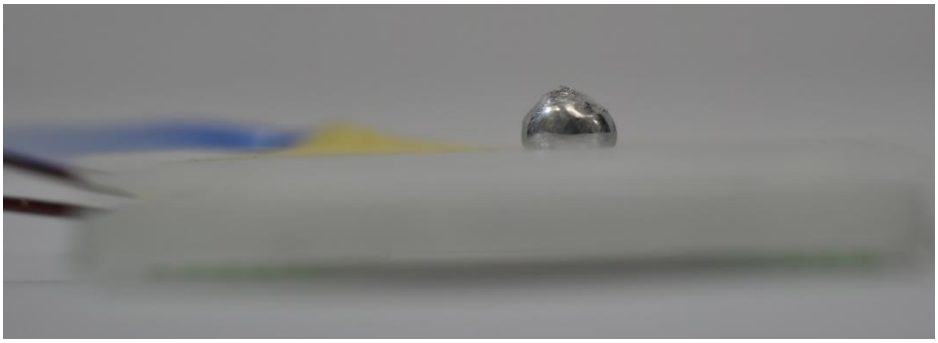

Figure 19: Wetting Experiment Sample Example

The images in the droplets were all loaded into a program to take 5 angle measurements of each droplet side. The accumulated measurements can be seen below in Table 3. The average of these angle measurements were calculated to be 132.49° at the average temperature of 77°C . This is very comparable to angle the silicon droplets performed in the experiment by Hideyuki Kanai at 1550°C ((Kanai et al., 2007)). At 1500°C, the silicon droplets on quartz produced a wall angle of 130° in the stated research. This value gives promising results that the surface tension of silicon will act similarly to alloy U-72 when crucibles for silicone are set to the proper environment at temperature.

Table 3: Wetting Experiment Measurements and Average Angle

rigth side of picture								
Measurement #	1	2	3	4	5	AVE		AVE [°]
sample 1	139.28	131.25	139.51	132.08	140.3	136.484		132.49
sample 2	123.87	125.25	124.4	124.97	123.29	124.356		
sample 3	133.06	134.3	132.65	134.51	133.09	133.522		
sample 4	123.12	131.02	115.3	121.7	121.64	122.556		
sample 5	129.93	129.98	128.21	127.68	125.51	128.262		
left side of picture								
Measurement #	1	2	3	4	5	AVE		
sample 1	134.96	133.13	133.8	132.7	6 times	133.6475		
sample 2	131.96	134.37	136.07	131.58	7 times	133.495		
sample 3	117.17	120.22	116.66	116.47	8 times	117.63		
sample 4	132.54	139.59	139.62	132.08	9 times	135.9575		
sample 5	156.52	159.74	159.01	160.7	10 times	158.9925		

4.3 Solidification Experiment Results

Between the dates of October 13th and November 31st, the Solidification lab from SIT produced 37 U-72 alloy substrates following the general process stated in the methodology. Throughout the experiments, the variables like voltage, motor speed, and the forced cooling rate were altered to get a better understanding for which had the highest effect on the substrate quality. Figure 20 displays 6 chosen experiment substrates: three under 630 kHz (a) and three under the 2.5 MHz (b) conditions. They were chosen to display some of the ideal characteristics that have been seen is successful substrates, while also being able to highlight some of the faults that appear when factors like voltage and air-cooling rate are changed.

Figure 20: Examples of Successful Alloy U-72 Substrates at (a) 630 kHz and (b) 2.5 MHz

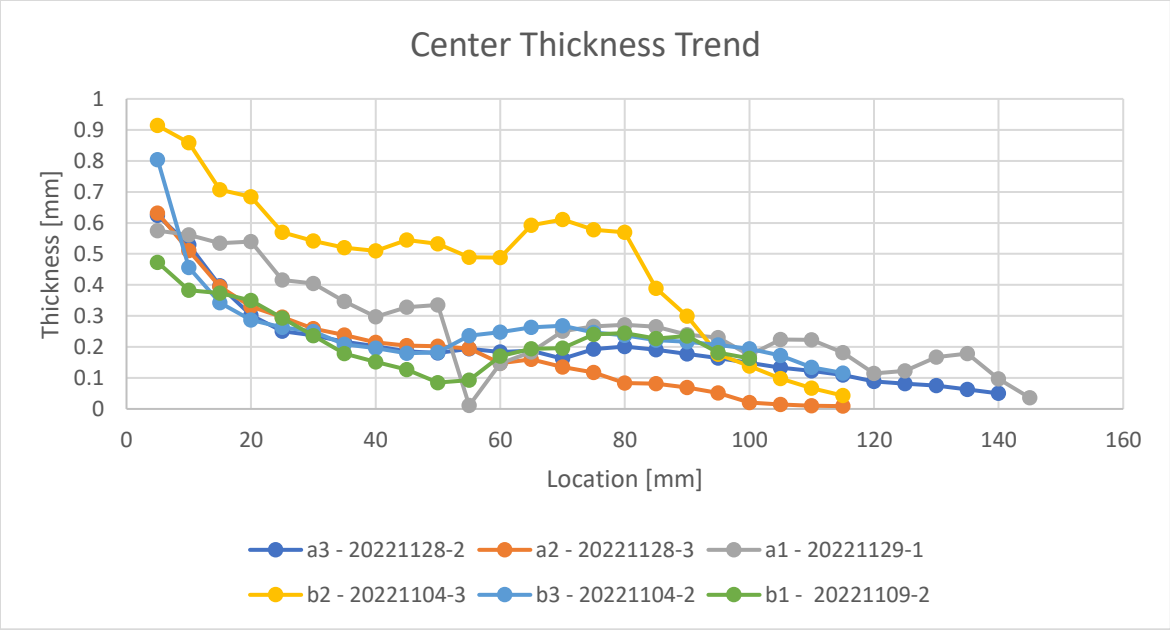

Figure 21: Center Thickness Trend Chart from 20 Samples

As seen above in Figure 21, the variety of substrates is quite large. Due to the drop in thickness after the electromagnetic pressure is applied sample a2 shows favorable characteristics through its consistency of areas of thin thickness and its stability over the last 40mm. Similar substrates that decrease in thickness initially often sever from the crucible within 5-10mm after the electromagnetic pressure is applied. Sample a2 was ran so that the cooling rate was manually adjusted to center the solidification line after the initial values from the ANSYS was used. This was so the team could properly monitor and react to the changing position of the solidification line of the forming substrate. This is suspected to aid the substrate from severing its connection to the crucible due to an aggressive solidification line, or inversely to prevent the substrate from not being affected by the electromagnetic pressure with a lagging solidification line. In the future of this research, the process of monitoring and adjusting the solidification line should be automated to avoid human error.

A reoccurring result in many substrates showed an immediate decrease in thickness 5-10 mm after the introduction of the electromagnetic current, followed by a rapid increase in thickness 5-10 mm later. Samples a1, b1, and b2 from Figure 20 as well as Figure 22 and Figure 23 showed this trend. What the

research team deduced was that the immediate effect of turning on the electromagnetic pressure coils displaced some of the liquid alloy back into the crucible pushing back the solidification line. This caused the immediate area to be thinned, but the following region on the substrate dealt with a slightly higher level of liquid alloy solidified before it reached the proper area under the coils. The most extreme example of this phenomena can be seen in Figure 21 a1.

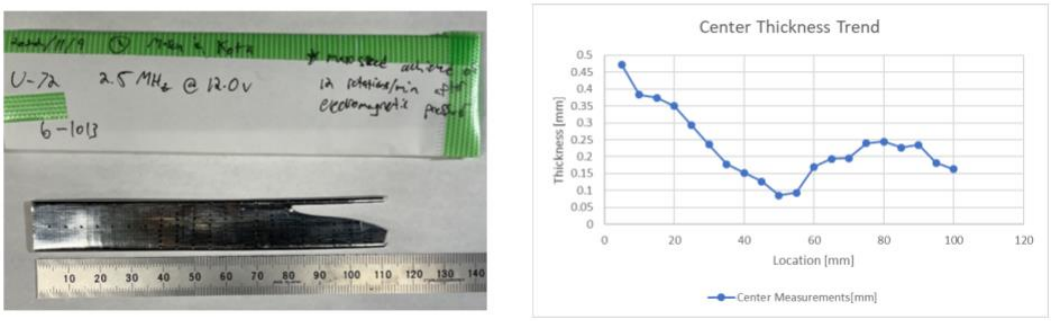

Figure 22: Sample 2022119-2 Displaying Rapid Increase of Thickness

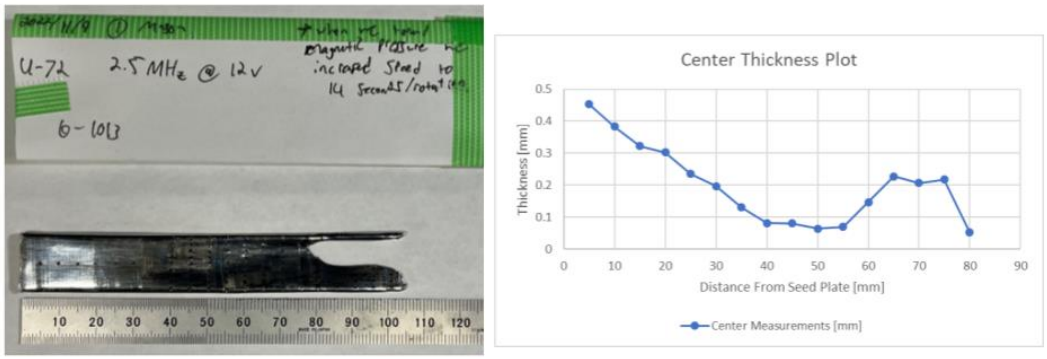

Figure 23: Sample 2022119-1 Displaying Rapid Increase of Thickness

Below in Figure 24 is a visualization of the thickness across sample 20221109-3 also seen in Figure 20 - a2. These plots were generated for the majority of the successful substrates produced. This one in particular highlights all of the near 100 micrometer thick sections in dark red. You can see that the first application of the electromagnetic pressure develops a thickness near the desired level, then jumps back up nearly 100 micrometers on average per section.

Sample 20221108-3	Position From Center									
Distance From Seed Plate [mm	-9	-8	-6	-4	-2	0	2	4	6	8	9
[mm]_45mm		0.433	0.454	0.485	0.517	0.487	0.467	0.403	0.548	0.855	
[mm]_55mm		0.375	0.227	0.287	0.25	0.225	0.186	0.156	0.108	0.843	
[mm]_65mm		0.44	0.26	0.268	0.329	0.306	0.269	0.23	0.282	0.821	
[mm]_75mm		0.473	0.289	0.262	0.276	0.33	0.302	0.263	0.278	0.894	
[mm]_85mm		0.375	0.255	0.266	0.299	0.306	0.29	0.248	0.422	0.903	
[mm]_95mm		0.345	0.223	0.228	0.289	0.283	0.24	0.221	0.357	0.822	
[mm]_105mm		0.253	0.184	0.207	0.288	0.236	0.197	0.172	0.337	0.815	
[mm]_115mm		0.3	0.168	0.158	0.27	0.228	0.183	0.151	0.243	0.811	
[mm]_125mm		0.283	0.127	0.134	0.215	0.187	0.118	0.127	0.204	0.802	
[mm]_135mm		0.302	0.114	0.143	0.252	0.194	0.113	0.106	0.254	0.752	
[mm]_145mm		0.321	0.106	0.107	0.199	0.156	0.106	0.112	0.222	0.721	
[mm]_155mm		0.258	0.076	0.06	0.169	0.133	0.05	0.041	0.193	0.703	
[mm]_165mm		0.362	0.045	0.041	0.128	0.013			0.158	0.667	
[mm]_175mm		0.227	0.004	0.015	0.1					0.625	
[mm]_185mm		0.163			0.147						
[mm]_195mm		0.304			0.182						
[mm]_205mm											
[mm]_215mm											

Figure 24: Thickness Visualization of Sample 20221109-3

5.0 Discussion

The research experiments described pertain strictly to the use of alloy U-72 and its thermal properties in the creation of ultra-thin substrates. Although pure Silicon is not used, these findings can support a foundation to further investigate it's implementation into the production of ultra-thin Silicon wafers.

5.1 Successful Experiments Creating Ultra-Thin Alloy Substrates

The experiments utilizing 2.5 MHz and 630 kHz electromagnetic frequencies to create ultra-thin substrates of the alloy U-72 can be deemed successful. The majority of the samples, despite the variety of conditions, displayed rapidly decreased thicknesses after the electromagnetic pressure was applied. There were also larger areas of decreased thickness compared to past research samples.

There still remained inconsistencies from planned and unexpected variables that plagued many of the samples. For instance, the experimental test rig routinely had leveling issues. Every few days a

string of samples severed the substrate heavily on one side particular side. This can be seen in the samples from Figure 22 and Figure 23 displaying a large gap before the end of the sample. When the experiment test rig is properly serviced these kinds of issues can be mitigated. Stronger washer and nut combinations or dampening the feet of the rig to avoid excess chatter are two ways to mitigate the changing of leg height of the rig over time. Once this issue was noticed, it was addressed and marked in the notes on the next sample.

Monitoring the liquid level of the crucible was another factor that had direct impact on the quality of substrates produced. If the crucible was not properly refilled after a successful substrate was generated, the lower level of the liquid alloy would sever the substrate before the start of the electromagnetic pressure, ending the experiment. When the crucible was overfilled with liquid alloy the substrates produced often had difficulties getting below a thickness of 200 micrometers. adding a level line to the next version of the crucible is a quick way to validate that the amount of liquid within is correct.

The largest factor for premature failure that was briefly mentioned in the results was the voltage of the electromagnetic pressure coils. 2.5 MHz at 12 volts was found to be very consistent when making substrates, however the initial conditions of 630 kHz at 8 volts had much more varying results. When failures occurred directly after the pressure was applied the reasoning was usually one of two assumptions; 1) the solidification line was too far forward due to a low forced heat transfer rate from the cooling air, or 2) the immediate pressure applied overpowered the liquids surface tension severing the substrate from the crucible. To investigate the second issue the team devised a series of supplemental experiments adjusting the voltages for the 630 kHz condition.

By varying the voltage ±2 volts from the original condition of 6 volts, 5 volts was found to be a more optimal force to thin the substrate without separating it. Figure 25 was created after testing that

result and displays the trend of the center thickness through the length of the substrate. It shows a thickness below 100 micrometers throughout a large area past the line where the electromagnetic pressure was applied. Figure 26 shows, in more detail, the large amount of area the that is near or below the ideal thickness of 100 micrometers in deep red. Since that week This sets our ideal initial conditions for the experiment using 2.5 MHz at 12 volts and 630 kHz at 5 volts so the electromagnetic pressure can consistently create the best thinned U-72 substrates.

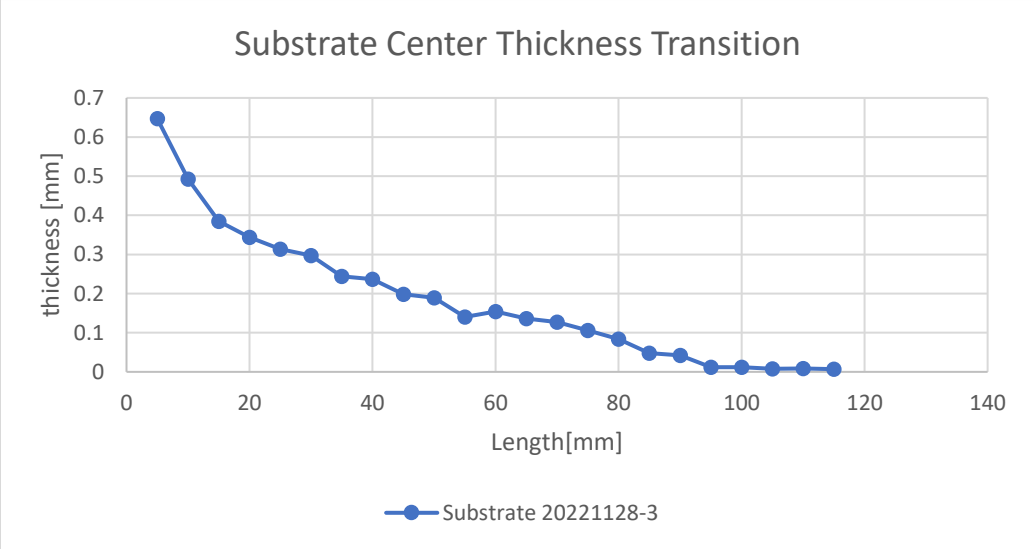

Figure 25: Substrate Produced Under Ideal Conditions

	distance from center (mm)										
length after pressure is applied (mm)	-9	-8	-6	-4	-2	0	2	4	6	8	9
45		0.347	0.304	0.242	0.231	0.198	0.145	0.167	0.143	0.296	
50		0.299	0.288	0.256	0.224	0.189	0.123	0.146	0.0143	0.524	
55		0.245	0.225	0.208	0.168	0.14	0.077	0.085	0.17	0.512	
60		0.237	0.254	0.209	0.181	0.154	0.081	0.107	0.142	0.381	
65		0.246	0.23	0.215	0.164	0.136	0.098	0.108	0.197	0.434	
70		0.204	0.213	0.198	0.15	0.127	0.073	0.097	0.202	0.396	
75		0.194	0.2	0.18	0.127	0.106	0.056	0.061	0.189	0.388	
80		0.177	0.167	0.139	0.106	0.084	0.034	0.05	0.174	0.355	
85		0.138	0.144	0.12	0.085	0.048	0.012	0.039	0.154	0.349	
90		0.15	0.144	0.099	0.075	0.042	0.009	0.034	0.117	0.322	
95		0.111	0.107	0.082	0.039	0.012	0.007	0.016	0.133	0.303	
100		0.113	0.106	0.072	0.03	0.012	0.009	0.013	0.159	0.303	
105		0.121	0.093	0.03	0.018	0.008	0.006	0.01	0.134	0.303	
110		0.114	0.061	0.01	0.008	0.009	0.007	0.011	0.13	0.303	
115		0.103	0.095	0.042	0.009	0.007	0.007	0.008	0.135	0.303	
120		0.105	0.102	0.041	0.01					0.303	
125		0.106	0.144								
130		0.145									

Figure 26: Substrate 20221128-3 Full Thickness Measurements

5.2 Discussion comparing Alloy U-72 to Silicon

For future research, this experimental model needs successful replicability with pure silicone to prove the viability as a new manufacturing process for photovoltaic silicon wafers. The similarities for heat transfer, surface tension, and electromagnetism are favorable characteristics which back the hypothesis that silicon is a viable material for this type of experimental process. The comparison of these values can be seen in Table 2 from section 4.2. This table displays the correlation of the similar material properties as well as the dimensionless characteristics like the Weber number and Magnetic Reynolds Number. It is expected that the surface tension and liquid flow of silicon would react similarly to the U-72 alloy in these experiments. That being said, the stability of liquid silicon and the silicon transition from liquid to solid would require different considerations when designing the cooling system and experimental setup for this material. Although it would require an automated system in an air tight atmosphere, it is believed that the basis of this experiment can be replicated on silicon.

5.3 Broader Impacts

Due to the large need for renewable energy resources in the near future, research pushing the limits in the industry is often encouraged and subsidized. Although in its early stages, this research has the ability to encourage change in the photovoltaic manufacturing market, increasing competition with modern processes, driving down the barrier for entry into the utilization for solar energy. If the proposed process for thinning silicon wafers can be achieved, manufacturing cost and expenditures related to production should decrease (Liu et al., 2020). Since 2012, there has been a positive correlation between government subsidization on photovoltaics R&D, and the instillation of photovoltaic systems (Shao & Fang, 2021). Similar trends can be seen throughout history for nearly all kinds of products. The first consumer color televisions hit the market at over $7,000 adjusted for modern inflation. Today, a 60-inch 4K HD television can cost around $300 - $500. This trend has followed many technologies through the ages from phones to microelectronics. As the research continues within the industry competition will arise, advancements will be made, efficiencies will increase, the cost of entry will drop, and more people and business will turn to the use of solar energy. This future will improve the wellbeing of individuals within society by preventing the negative effects of climate change and decreasing the cost of electricity for the general consumer.

6.0 Conclusion

This research study has been successful at utilizing electromagnetic pressure to thin the alloy U-72 substrates over larger areas comparing to previous studies. The best quality substrates were produced with conditions at 2.5MHz with 12 volts as well as 630 kHz with 5 volts. These main condition variables were the largest factor that effected the quality of the produced substrates. If the voltage was

too high the substrates were more likely to be severed from the liquid melt. If the voltage was too low the substrate would not experience enough force to be sufficiently thinned.

When comparing U-72 to silicon, the material properties have similar values and orders of magnitudes leading the team to believe silicon can be a viable material for thinning continuous wafers with electromagnetic pressure. The wetting experiment comparisons generated further results to add confidence to this hypothesis. Overall, the use of electromagnetic pressure for thinning specific alloy substrates has been seen to be successful. The next stages of this research should validate the use of silicon or other similar metallic materials to further prove the need for higher level research and investigation at a larger scale.

Bibliography

"Best Research-Cell Efficiency Chart." Accessed December 1, 2022. https://www.nrel.gov/pv/cell-efficiency.html.

Bloch, Michael. "Thinner Solar Cells = Even Cheaper Solar Panels? SolarQuotes Blog." Solar Quotes Blog, January 27, 2020. https://www.solarquotes.com.au/blog/thinner-solar-cells-mb1384/.

"Chapter I-1-A. Principles of Solar Cell Operation | Elsevier Enhanced Reader." Accessed November 8, 2022. https://doi.org/10.1016/B978-0-12-809921-6.00001-X.

Fraas, Lewis M. "History of Solar Cell Development." In *Low-Cost Solar Electric Power*, edited by Lewis M. Fraas, 1–12. Cham: Springer International Publishing, 2014. https://doi.org/10.1007/978-3-319-07530-3_1.

Goetzberger, Adolf, Christopher Hebling, and Hans-Werner Schock. "Photovoltaic Materials, History, Status and Outlook." *Materials Science and Engineering: R: Reports* 40, no. 1 (January 1, 2003): 1–46. https://doi.org/10.1016/S0927-796X(02)00092-X.

Hanoka, Jack I. "An Overview of Silicon Ribbon Growth Technology." *Solar Energy Materials and Solar Cells* 65, no. 1–4 (January 2001): 231–37. https://doi.org/10.1016/S0927-0248(00)00154-9.

American Chemical Society. "How a Solar Cell Works." Accessed November 9, 2022. https://www.acs.org/content/acs/en/education/resources/highschool/chemmatters/past-issues/archive-2013-2014/how-a-solar-cell-works.html.

Kanai, Hideyuki, Sunao Sugihara, Hiroshi Yamaguchi, Tomonori Uchimaru, Naoyuki Obata, Toshiyuki Kikuchi, Fusaki Kimura, and Masato Ichinokura. "Wetting and Reaction between Si Droplet and SiO2 Substrate." *Journal of Materials Science* 42, no. 23 (December 1, 2007): 9529–35. https://doi.org/10.1007/s10853-007-2090-z.

Liu, Binguo, Jinghui He, Xiangrui Cao, Chao Yan, Zhi Cheng, Ruiqiang Huang, Zijiang Zhou, Qin Liu, and Xiaopu Fan. Production method of solar grade czochralski monocrystalline silicon. CN104328494 (A), issued February 4, 2015. https://worldwide.espacenet.com/publicationDetails/biblio?FT=D&date=20150204&DB=EPODOC&locale=&CC=CN&NR=104328494A&KC=A&ND=2.

Liu, Zhe, Sarah E. Sofia, Hannu S. Laine, Michael Woodhouse, Sarah Wieghold, Ian Marius Peters, and Tonio Buonassisi. "Revisiting Thin Silicon for Photovoltaics: A Technoeconomic Perspective." *Energy & Environmental Science* 13, no. 1 (2020): 12–23. https://doi.org/10.1039/C9EE02452B.

Majumdar, G., M. Chakraborty, and M. S. J. Hashmi. "Fine Grinding of Semiconductor Materials: Review of Past and Current Practices." In *Reference Module in Materials Science and Materials Engineering*. Elsevier, 2016. https://doi.org/10.1016/B978-0-12-803581-8.04146-1.

Markvart, Tom, and Luis Castañer. "Chapter I-1-A - Principles of Solar Cell Operation." In *McEvoy's Handbook of Photovoltaics (Third Edition)*, edited by Soteris A. Kalogirou, 3–28. Academic Press, 2018. https://doi.org/10.1016/B978-0-12-809921-6.00001-X.

Ohno, A. “Continuous Casting of Single Crystal Ingots by the O.C.C. Process.” *JOM* 38, no. 1 (January 1, 1986): 14–16. https://doi.org/10.1007/BF03257948.

Rossi, Cesare, and Flavio Russo. *Ancient Engineers’ Inventions*. Vol. 33. History of Mechanism and Machine Science. Cham: Springer International Publishing, 2017. https://doi.org/10.1007/978-3-319-44476-5.

Shao, Xuefeng, and Tianshu Fang. “Performance Analysis of Government Subsidies for Photovoltaic Industry: Based on Spatial Econometric Model.” *Energy Strategy Reviews* 34 (March 1, 2021): 100631. https://doi.org/10.1016/j.esr.2021.100631.

Stankovic, Sinisa, Neil Campbell, and Alan Harries. *Urban Wind Energy*. London: Routledge, 2009. https://doi.org/10.4324/9781849770262.

Stefano, Meroli. “Silicon vs Graphene. The Future of Electronics and Microelectronics.” Accessed November 9, 2022. https://meroli.web.cern.ch/www.cern.ch/meroli/lecture_meaning_discovery_czochralski.html.

Appendix

List of Figures

List of Tables

Equations